M dwarfs in Sloan Digital Sky Survey Stripe 82: Photometric light curves and flare rate analysis

Citation: Kowalski, Adam F., Suzanne L. Hawley, Eric J. Hilton, Andrew C. Becker, Andrew A. West, John J. Bochanski, and Branimir Sesar. "M Dwarfs in Sloan Digital Sky Survey Stripe 82: Photometric Light Curves and Flare Rate Analysis." The Astronomical Journal 138, no. 2 (July 8, 2009): 633–648. © 2009 The American Astronomical Society

As Published: http://dx.doi.org/10.1088/0004-6256/138/2/633

Publisher: IOP Publishing

Persistent URL: http://hdl.handle.net/1721.1/92800

Version: Final published version: final published article, as it appeared in a journal, conference proceedings, or other formally published context

The Astronomical Journal, 138:633–648, 2009 August doi:10.1088/0004-6256/138/2/633

M DWARFS IN SLOAN DIGITAL SKY SURVEY STRIPE 82: PHOTOMETRIC LIGHT CURVES AND FLARE RATE ANALYSIS*

Adam F. Kowalski[1], Suzanne L. Hawley[1], Eric J. Hilton[1], Andrew C. Becker[1], Andrew A. West[2], John J. Bochanski[2], and Branimir Sesar[1]

[1] Astronomy Department, University of Washington, Box 351580, Seattle, WA 98195, USA; kowalski@astro.washington.edu
[2] MIT Kavli Institute for Astrophysics & Space Research, 77 Massachusetts Avenue, Building 37, Cambridge, MA 02139, USA
Received 2009 March 3; accepted 2009 June 10; published 2009 July 8

ABSTRACT

We present a flare rate analysis of 50,130 M dwarf light curves in Sloan Digital Sky Survey Stripe 82. We identified 271 flares using a customized variability index to search ∼2.5 million photometric observations for flux increases in the *u* and *g* bands. Every image of a flaring observation was examined by eye and with a point-spread function-matching and image subtraction tool to guard against false positives. Flaring is found to be strongly correlated with the appearance of Hα in emission in the quiet spectrum. Of the 99 flare stars that have spectra, we classify eight as relatively inactive. The flaring fraction is found to increase strongly in stars with redder colors during quiescence, which can be attributed to the increasing flare visibility and increasing active fraction for redder stars. The flaring fraction is strongly correlated with $|Z|$ distance such that most stars that flare are within 300 pc of the Galactic plane. We derive flare *u*-band luminosities and find that the most luminous flares occur on the earlier-type m dwarfs. Our best estimate of the lower limit on the flaring rate (averaged over Stripe 82) for flares with $\Delta u \geqslant 0.7$ mag on stars with $u < 22$ is 1.3 flares hr^{-1} deg^{-2} but can vary significantly with the line of sight.

Key words: methods: data analysis – stars: activity – stars: flare – stars: late-type

Online-only material: color figures

1. INTRODUCTION

Flares are a powerful manifestation of stellar magnetic fields, releasing stored energy from surface magnetic loops into the outer atmosphere of the star, and causing strong transient increases in the blue and ultraviolet (UV) continuum emission as well as in optical, UV, and X-ray emission lines. There are many unsolved problems in flare physics, ranging from the details of the energy release, to the mechanisms for producing the atmospheric emission, to the understanding of flares on a global scale—which stars flare, how often, how much emission do they produce, and on what timescales? In the past, the investigation of these global questions has been hampered by the need to obtain long time series observations of individual stars, which is an exceedingly time-consuming exercise involving both ground-based data (Moffett 1974; Lacy et al. 1976) and satellite data (Audard et al. 2000; Güdel et al. 2003). The advent of large time-resolved sky surveys covering a significant fraction of the sky (e.g., Pan-STARRS, Kaiser 2004; LSST, Tyson 2002; Ivezić et al. 2008; Gaia, Perryman et al. 2001) will provide an entirely new opportunity to assemble flare data from repeat observations of millions of stars on timescales of minutes to days. The analysis of these new data will be quite different from classical flare data which were obtained continuously on single objects.

In this paper, we use data from the Sloan Digital Sky Survey (SDSS; York et al. 2000) to perform an initial examination of the possibilities for studying flares in a large sky survey database. The SDSS contains repeat observations of one particular part of the sky, known as Stripe 82, along the celestial equator. This region was targeted because it is in the south Galactic hemisphere, and is visible from Apache Point Observatory during the northern autumn months (September–December) when the main SDSS fields in the north Galactic hemisphere are not accessible. The original motivation was to obtain numerous photometric scans of the same region of sky so that they could be co-added to produce a photometric template 1–2 mag deeper than the normal SDSS data and to quantify observational precision and repeatability. It was recognized early on, however, that the individual observations formed a valuable time sequence of data that could be mined to identify time-variable phenomena. Many additional SDSS-II scans of this region were also obtained as part of the SDSS-II Supernova Survey (Frieman et al. 2008). The Stripe 82 data products are contained in the SDSS Data Release 7 (Abazajian et al. 2009). An investigation aimed at characterizing flare signatures in the SDSS Stripe 82 data is therefore timely.

We have two primary goals in this paper. The first is to investigate flare frequencies as a function of spectral type and magnetic activity status, where active stars are defined as those with the chromospheric Hα line in emission. We restrict our investigation to low-mass stars, of spectral type M0 and later, and we also concentrate on identifying bona fide flares with high probability (rather than accepting lower probability events which may not be flares). Our previous photometric and spectroscopic studies of the m dwarfs in SDSS have revealed correlations of the active fraction with spectral type (later-type stars are more likely to be active) and with distance from the Galactic plane, such that stars closer to the plane are more likely to be active, and statistically are members of a younger population (West et al. 2004, 2008). The combination of these effects leads to the result that later-type stars maintain their activity for a longer time, perhaps for nearly the entire ∼10 Gyr lifespan of the Galactic disk, while early M dwarfs lose their activity in less than 1 Gyr (West et al. 2008). We wish to determine whether the stars that flare follow the same trends as the active stars, as would be expected from the standard model connecting flare emission with magnetic reconnection.

* Based on observations obtained with the Apache Point Observatory 3.5 m telescope, which is owned and operated by the Astrophysical Research Consortium.

The SDSS Stripe 82 data provide a unique sample with which to investigate these effects, since previous flare data have been obtained only during continuous monitoring of individual, nearby stars.

The second goal is to provide an initial set of flare frequencies as a function of spectral type and Galactic position to compare to our numerical simulations of flaring rates across the Galaxy (these simulations are in progress and will be reported in E. J. Hilton et al., 2009, in preparation). Our previous work on the mass and luminosity functions of the low-mass stars in the Galaxy (Covey et al. 2006, 2008b; Bochanski et al. 2007a, 2007b) together with our knowledge of the active fraction of M dwarfs as a function of Galactic height and spectral type, allows us to predict how many stars should be flaring at a given Galactic position during a given exposure time. Many of the parameters of such a global flaring model can only be roughly estimated at present, and the SDSS Stripe 82 sample will give us the opportunity to test whether the model is achieving reasonable agreement with the data.

The structure of the paper is as follows. We first describe the SDSS data set, and our sample selection which is designed to choose only those targets with trustworthy observations for analysis (Section 2). We then discuss in considerable detail our efforts to develop a flare variability index that can be applied uniformly to the time-resolved photometry to identify candidate flaring epochs (Section 3). The results of applying this flare variability index to the sample are discussed in Section 4, where we investigate the flare rates, correlation with spectral type, activity status, distance from the Galactic plane, and line of sight through the Galaxy. We also compare our flare luminosities and frequencies with previous determinations from nearby stars, and compare the flare rates with simple model predictions. In Section 5, we summarize our results.

2. DATA

The SDSS (York et al. 2000; Stoughton et al. 2002a; Pier et al. 2003; Ivezić et al. 2004) is a large (∼10,000 deg^2), multicolor (*ugriz*; Fukugita et al. 1996; Gunn et al. 1998; Hogg et al. 2001; Smith et al. 2002; Tucker et al. 2006) photometric and spectroscopic survey centered on the northern Galactic cap. The Sloan 2.5 m telescope (Gunn et al. 2006), located at Apache Point Observatory, operates in drift-scan mode as the camera (Gunn et al. 1998) simultaneously images the sky in five bands, yielding photometry of ∼287 million unique objects contained in the SDSS Data Release 6 (Adelman-McCarthy et al. 2008).

SDSS Stripe 82 is a narrow band comprising ∼300 deg^2 along the celestial equator ($-51^\circ < \alpha < +60^\circ$, $-1.266^\circ < \delta < +1.266^\circ$) that was observed more than 20 times under photometric conditions between 2001 and 2005. Many additional (40–60) SDSS-II imaging observations of Stripe 82 were obtained during 2005–2007; these data were not necessarily photometric and required additional processing (Ivezić et al. 2007). The catalog of photometric observations we use incorporates the Ivezić et al. (2007) calibrations, and was assembled as a queryable time-domain database at the University of Washington in Spring 2008, in advance of the date when the repeat Stripe 82 scans were released to the public as part of DR7 (2008 October; Abazajian et al. 2009).

2.1. Sample Selection

The following steps outline the process we used to identify a sample of M dwarfs from the SDSS Stripe 82 single epoch photometry (DR6), obtain their light curves (from the UW time-domain database, though these data are now available in DR7), and restrict the analysis to include only reliable, well-determined photometry. Note that in this section and in Section 3, we perform all analysis on the actual measured magnitudes (or fluxes) and their associated errors. In other parts of the paper when considering color–spectral type relations, distances, and luminosities, we apply interstellar reddening and extinction corrections to the measured magnitudes using the standard SDSS corrections contained in the photometric database, which are based on the dust maps from Schlegel et al. (1998).

1. The SDSS Data Release 6 was searched for point sources with the colors of low-mass stars in Stripe 82. Based on West et al. (2005) and Bochanski et al. (2007b), the color limits were chosen as $(r - i) > 0.53$ and $(i - z) > 0.3$ to restrict the sample to M stars. The initial sample comprised more than 1.4 million candidate objects.
2. The photometry in each of the r, i, z filters used to form the colors was required to be brighter than the survey limiting magnitudes. This reduced the sample to ∼900,000 candidate objects.
3. Standard SDSS photometry processing flags (Stoughton et al. 2002b) were used to reject objects due to poor DR6 single-measurement photometry. In particular, data were removed if any of the following flags were set: SATURATED, NODEBLEND, NOPROFILE, PSF _FLUX_INTERP, BAD_COUNTS _ERROR, INTERP_ CENTER, DEBLEND_NOPEAK, NOTCHECKED. The sample now contained ∼700,000 objects from one of the following SDSS Legacy runs: 2583, 2659, 2662, 2738, 3325, or 3388.
4. By far the most significant cut was the next one, where the u photometry was required to satisfy a brightness limit $u < 22.0$. The reason is that flares are most prominent in the u band, and if we cannot measure the quiet (outside of flaring) u magnitude accurately then we cannot compare the properties of flaring epochs relative to the quiet star. Because M dwarfs typically have $(u - r) > 3$, this effectively restricts the sample to stars with $r < 19$, which significantly decreases the volume over which the stars can be observed. Only ∼42,000 stars passed this cut.
5. The UW time-domain database was then employed to search for matches within 2″ of the DR6 position. Observations were kept if they had good astrometry, magnitude errors <1 mag, and good field-wide zero point measurements (important for data obtained under nonphotometric conditions). Only a few hundred stars failed this cut.
6. To determine the mean quiet (nonflaring) magnitude in each filter for each star, the measured magnitudes were first converted to fluxes (see Section 3.2), and a median flux was calculated for each filter. A 3σ (where σ is the median absolute deviation from the median) cut was then made, and the weighted mean flux (where each measurement is weighted inversely by the square of the photometric error) was determined for each filter, subject to the requirement that at least five epochs had photometry within 3σ available in each filter. Mean fluxes were formed for ∼41,000 stars. Figure 1 (left) plots the fraction (typically >60%) of the total number of photometric observations that was used to determine the mean flux for each star. Figure 1 (right) shows the number of good observations in the u and g filters (that is, the observations returned from the UW time-domain database as per step 5 above, but not necessarily good

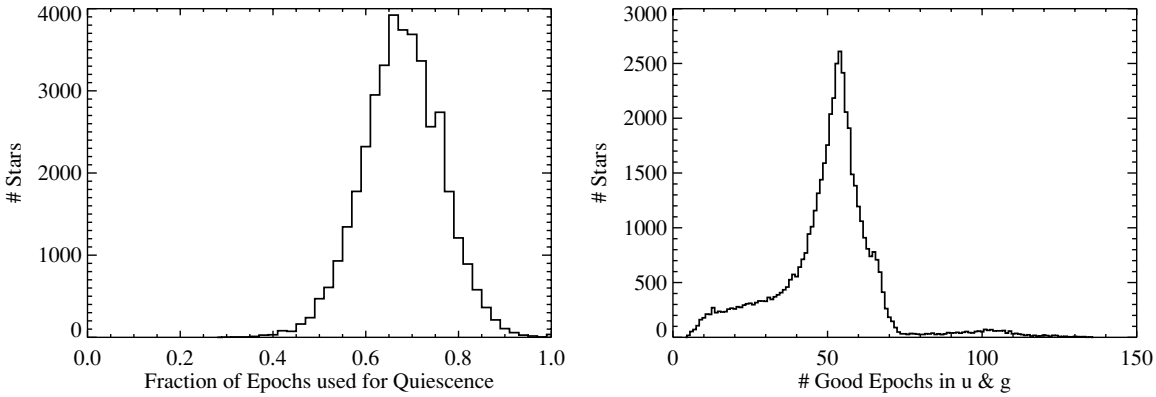

Figure 1. Left: the fraction of epochs used for the quiescent magnitude calculation shows that a significant number of observations were excluded due to being >3 median absolute deviations away from the median. Right: the number of good epochs per star in both the *u* and *g* filters.

according to the SDSS photometry flags). The leftmost asymmetry is caused by stars that have $u > 21.7$ and therefore straddle the detection limit in the *u* band. The peak near 100 observations is due to the stars that lie in the overlap regions of camera columns between the N and S components of Stripe 82, and therefore were observed twice as many times.

7. To ensure that the colors calculated from the light curves are consistent with the initial DR6 color cut (see step 1 above), the same color cut was applied to the mean quiet magnitudes, reducing the sample by a few hundred stars.[3]
8. A color cut requiring that $u - g > 1.8$ (Smolčić et al. 2004) was applied to eliminate ∼600 potential unresolved white dwarf–M dwarf binaries, which have bluer $u - g$ colors. The frequency of M dwarf–M dwarf binaries is likely ∼35% (Fischer & Marcy 1992; Reid et al. 2002). Unresolved M dwarf binaries add uncertainty to the analysis, since the color of the star may not give an accurate quiescent luminosity and distance. However, it is not possible to eliminate unresolved M dwarf–M dwarf binaries using photometry alone. Our final *ugriz* sample consists of 39,633 stars with observations totaling 1,987,253 epochs.
9. An additional photometric sample was obtained by following the prescription above for stars with reliable *ug* photometry, but *riz* photometry that is saturated, or faulty in another way. Starting with $u < 22$, $u > g$, and more stringent magnitude requirements for the *u* and *g* bands (magnitude errors ⩽0.1), an additional ∼500,000 point sources were obtained from the DR6 catalog in Stripe 82. Matching to the Two Micron All Sky Survey (2MASS) within 2″, requiring good *K*-band photometry (signal-to-noise ratio (S/N) >5, magnitude error <0.1) and applying the color cuts $g - K > 4$ and $u - g > 1.8$ leaves ∼12,000 stars.[4] Matching to the time-domain database within 2″, and requiring well-defined quiet magnitudes (see step 6, above), gives the *ug*-only sample of 10,497 stars (524,981 epochs). Although we initially analyzed the two samples separately, the results were very similar and showed no systematic bias due to the lack of *riz* colors for the *ug*-only sample. Therefore, the rest of the analysis is shown for the combined sample.

[3] After correcting for interstellar reddening and extinction the limiting $r - i$ color was reduced to 0.43 and the limiting $i - z$ color to 0.23.

[4] After correcting for interstellar reddening and extinction the limiting $g - K$ color was reduced to 3.6.

2.2. Spectroscopic Observations and Spectral Types

About 10% of the stars (4005, comprising 197,867 epochs) in the *ugriz* photometric sample have SDSS spectroscopic observations, determined by matching to the spectroscopic DR6 database. None of the *ug*-only sample have SDSS spectra (these stars had poor *riz* photometry and therefore were likely rejected by the spectroscopic targeting algorithm). The stars with SDSS spectra have been assigned types using the Hammer spectral typing facility (Covey et al. 2007) and have been previously analyzed for magnetic activity based on detecting emission in the chromospheric Hα line (West et al. 2008). Stars characterized as *active* and *weakly active* by West et al. (2008) comprise the active sample (219 stars), with the rest of the spectroscopically observed stars being labeled inactive (3786 stars).

The vast majority of stars in our sample do not have spectra, so we assign an estimated spectral type based on the photometric colors. The estimated spectral types serve as a proxy for mass and surface temperature and provide a convenient way to subdivide the sample into intuitive "early, mid, late" spectral type bins to guide the analysis and compare to M dwarfs which do not have SDSS photometry. The colors used to assign types must first be corrected for extinction in order to avoid the common problem of assigning a reddened, early-type star at large distance an erroneous later spectral type, which would in turn place it at an (incorrect) closer distance. Since Stripe 82 is located in the southern Galactic hemisphere, our line of sight to nearly all stars (except the very closest) passes through the plane of the Galaxy. We therefore account for the interstellar reddening and extinction as described in Section 2.1.

The $(r - i, i - z)$ color–color diagram was used to classify the *ugriz* sample. We fit two-dimensional Gaussian distributions using FastMix (Moore 1999) to the West et al. (2008) DR5 M dwarf spectroscopic sample comprising some 20,000 stars with good *riz* colors and accurate spectral types based on SDSS spectra.[5] The resulting best-fit parameters (mean and covariance matrices, given in Table 1) define a two-dimensional Gaussian probability function for each spectral type, allowing us to assign estimated spectral types based on the photometric colors, as shown in the top panel of Figure 2.

For the *ug*-only sample, we estimate the spectral types according to the $g - K$ color (Covey et al. 2008b). Again using

[5] We augmented the original DR5 sample with additional M0 stars having bluer colors in order to fit the full color range of the extinction-corrected colors in our sample.

Table 1
M Dwarf Colors and Spectral Types

Spectral Subtype	μ	Σ
M0	(0.55, 0.32)	$\begin{pmatrix} 0.0159 & 0.0039 \\ 0.0039 & 0.0083 \end{pmatrix}$
M1	(0.78, 0.43)	$\begin{pmatrix} 0.0135 & 0.0051 \\ 0.0051 & 0.0055 \end{pmatrix}$
M2	(0.95, 0.52)	$\begin{pmatrix} 0.0163 & 0.0061 \\ 0.0061 & 0.0058 \end{pmatrix}$
M3	(1.15, 0.62)	$\begin{pmatrix} 0.0204 & 0.0076 \\ 0.0076 & 0.0076 \end{pmatrix}$
M4	(1.41, 0.76)	$\begin{pmatrix} 0.0213 & 0.0086 \\ 0.0086 & 0.0085 \end{pmatrix}$
M5	(1.87, 1.03)	$\begin{pmatrix} 0.0183 & 0.0084 \\ 0.0084 & 0.0062 \end{pmatrix}$
M6	(2.09, 1.14)	$\begin{pmatrix} 0.0194 & 0.0072 \\ 0.0072 & 0.0054 \end{pmatrix}$
M7	(2.49, 1.35)	$\begin{pmatrix} 0.0270 & 0.0107 \\ 0.0107 & 0.0095 \end{pmatrix}$

Notes. The best-fit parameters at each M dwarf spectral type for each two-dimensional Gaussian distribution of $r-i$, $i-z$ colors, determined from 20,000 M dwarfs in the West et al. (2008) DR5 spectroscopic sample with well-measured colors and well-determined types. Σ is the covariance matrix and is of the form $\Sigma = \begin{pmatrix} \sigma^2_{r-i} & \sigma_{r-i,i-z} \\ \sigma_{r-i,i-z} & \sigma^2_{i-z} \end{pmatrix}$. The probability for each spectral type is evaluated as $p(x) = \frac{1}{2\pi \|\Sigma\|^{1/2}} \exp(-\frac{1}{2}(\mathrm{x}-\mu)^{\mathrm{T}}\Sigma^{-1}(\mathrm{x}-\mu))$, $\mu = \begin{pmatrix} \mu_{r-i} \\ \mu_{i-z} \end{pmatrix}$ are the mean colors for a given type, and x are the $r-i$, $i-z$ colors for a given star.

the DR5 M dwarf spectroscopic sample, with K magnitudes from 2MASS, a one-dimensional Gaussian probability function for the extinction-corrected $g-K$ color was determined for each M spectral type. The bottom panel of Figure 2 shows the distribution of $r-i$ versus $g-K$ indicating that both colors provide reasonable estimates of the spectral type.

The dotted line in the top panel of Figure 3 gives the estimated spectral type distribution of the photometric (combined *ugriz* and *ug*-only) sample. The effect of the limiting apparent magnitude of the sample ($u < 22$) is clearly evident through the relatively large numbers of early-type (M0–M1) stars which can be seen to larger distances, and the small numbers of later-type (M4+) stars which can only be observed nearby. Therefore, the later-type stars come from a much smaller volume than the early-type stars. The colored lines in Figure 3 show the distributions of active and inactive stars as a function of spectral type. As expected (West et al. 2004), most of the early-type M dwarfs are inactive, while most of the later ones are active.

Finally, we investigated the contamination by giants in the sample. Separating giant and dwarf stars without high-resolution spectra is problematic. Covey et al. (2008b) examined the J versus $i-J$ color–magnitude diagram of two calibration regions (1 deg^2 each) in Stripe 82. We verified that the colors of the stars in our sample lie in the region of this color–magnitude diagram with <2% contamination from giants.

2.3. Follow-Up Spectra from the ARC 3.5 m Telescope

Time-domain survey data potentially allows the investigation of flaring rates from both active and inactive stars. The former have been well studied for many years, but the latter have received very little attention. Because we now have available a sample of "stars that flared," it is interesting to know if they are active or inactive in their quiescent state. Therefore, we obtained follow-up spectra with the ARC 3.5 m telescope at Apache Point

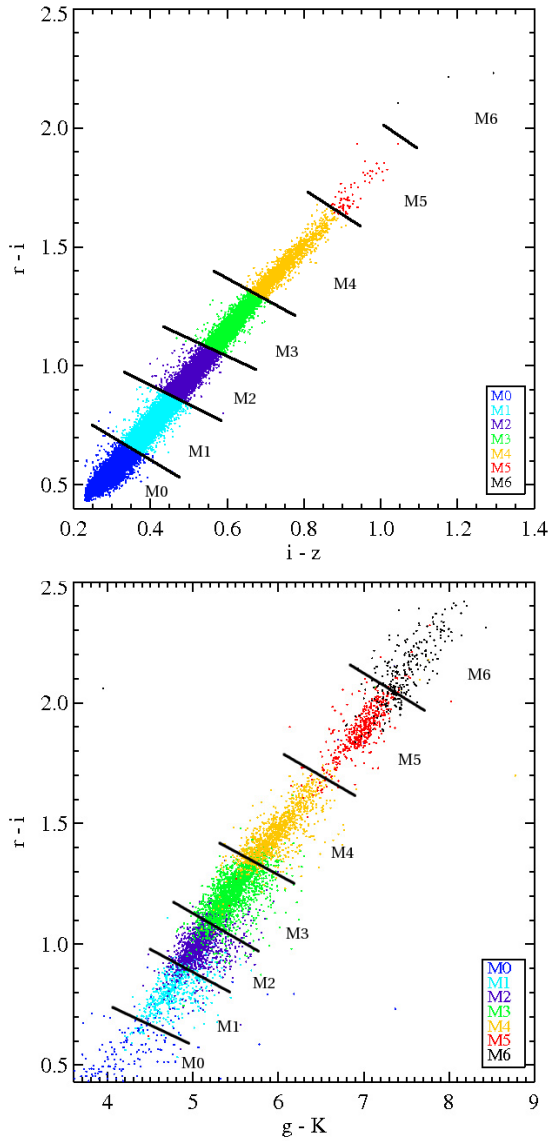

Figure 2. Top: the extinction-corrected $r-i$ vs. $i-z$ color–color diagram for the sample of 39,633 M dwarfs with well-defined light curves. The spectral types were probabilistically assigned based on our presented spectral type–color relations (Table 1). Bottom: the extinction-corrected $r-i$ vs. $g-K$ distribution of ~7200 stars with good photometry from the SDSS DR5 spectroscopic sample (West et al. 2008). Using this sample, we derive the mean and standard deviation of $g-K$ for each spectral type, which allows us to estimate the spectral types of the *ug*-only sample.

(A color version of this figure is available in the online journal.)

Observatory, using the Dual Imaging Spectrograph (DIS) with the R300 grating giving wavelength coverage ~6000 Å–9200 Å. On UT080825, we used a 2.″0 slit giving $R \sim 800$ and on the dates UT080919, UT081013, UT081107, UT081124, and UT081214 we used a 1.″5 slit giving $R \sim 1000$. As these stars are quite bright in r, exposures of 3–15 minutes gave S/N > 10 at Hα. Blue spectra were also obtained; however, the S/N was inadequate to obtain information about the activity status of the other H Balmer lines or Ca II H and K. The data were reduced using standard IRAF[6] procedures, wavelength

[6] IRAF is distributed by the National Optical Astronomy Observatories, which are operated by the Association of Universities for Research in Astronomy, Inc., under cooperative agreement with the National Science Foundation.

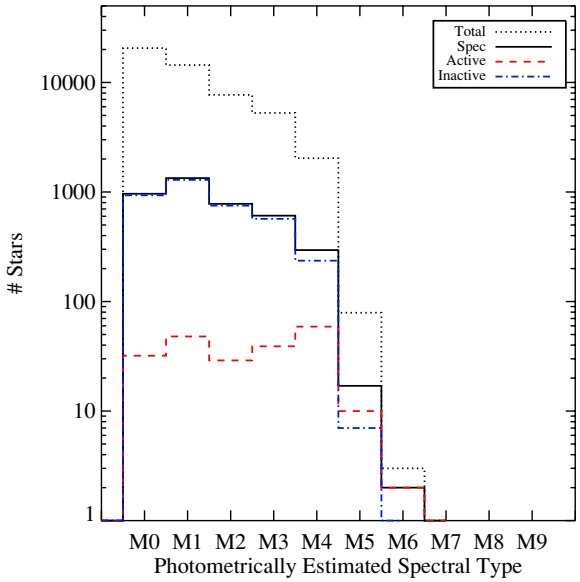

Figure 3. Distribution of M dwarfs sorted by the photometrically estimated spectral type for the total photometric sample (50,130 stars), the total spectroscopic sample (4005 stars), the active stars (219 stars), and the inactive stars (3786 stars).

(A color version of this figure is available in the online journal.)

calibrated using HeNeAr lamp spectra, and flux-calibrated using spectrophotometric standard star observations (though some of the data were taken during nonphotometric conditions, limiting them to a relative flux calibration). We discuss these observations further in the context of the relative probability of flares on active and inactive stars in Section 4.6.

3. VARIABILITY ANALYSIS

3.1. Properties of Flare Photometry

The SDSS Stripe 82 photometry for each M dwarf typically consists of ∼50 good observations (Figure 1), irregularly spaced in time with separation of several days, during the fall months, spanning several years. These data allow us to construct a low-cadence light curve in each filter. Since flaring timescales range from minutes to hours, individual flares will be observed only once during their time evolution. Therefore, each epoch of each star must be analyzed for a flare signature. An example of the *ugriz* light curves for an active M6 dwarf is shown in Figure 4. This star flared (with increases[7] of 5.5 mag in the *u* band, and 3.1 mag in the *g* band) during the first epoch marked with a star and again at much lower levels in the second marked epoch.

Flare emission can change significantly over the timescale of the SDSS photometric observations, which comprise ∼54 s in each filter as the star passes across the detector, in the filter order *r*–*i*–*u*–*z*–*g*. For the *u* and *g* observations which are primarily of interest here, this means that the *g* observation begins 108 s after the *u* observation, and there is a 54 s gap between them. Figure 5 illustrates the photometry measurements for a small flare, with a 0.6 mag increase at the peak in the *U* band (similar to *u*) and a 0.1 mag increase in the *B* band (similar to *g*), obtained with the NMSU 1 m telescope during 2008 April (A. F. Kowalski et al., 2009, in preparation). Depending on the timing of the SDSS

[7] Although increases in flux correspond to negative changes in magnitudes, to avoid confusion we refer to flares as having positive magnitude changes $\Delta u = |u_{\rm flare} - u_{\rm quiet}|$ throughout the paper.

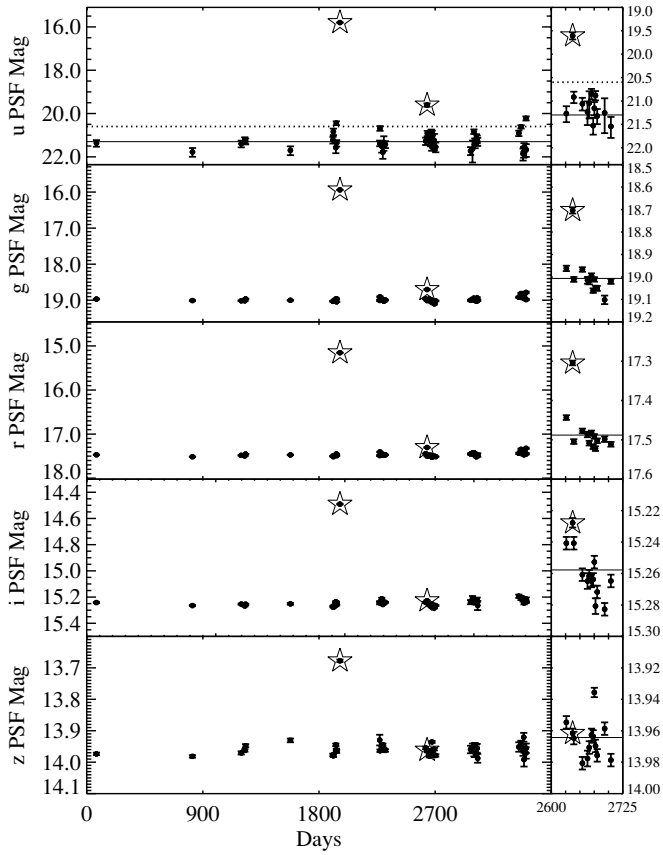

Figure 4. Example light curve with 46 observations in *ugriz* for an active M6 dwarf which exhibits both a large and small flare in the Stripe 82 data set (highlighted with star symbols). The magnitude enhancements for the large flare are Δmag= 5.50, 3.07, 2.34, 0.77, 0.29 in *ugriz*, respectively. Note that the small flare shows negligible enhancements in *i* and *z*. The inherent large variations in the *u* band necessitate our requirement for a simultaneous enhancement in the *g* band. The panels to the right zoom in on 13 observations (over 78 days) around the small flare. The solid line indicates the quiescent magnitude whereas the dotted line shows the 0.7 mag flare detection threshold.

observations obtained during such a flare, our requirement that both the *u* and *g* bands show enhancements (as described in the next section) would inefficiently select flares of this size. This is one of the reasons that we limit our flare detection capability to only those events that show 0.7 mag or larger increases in the *u* band (see Section 3.3).

3.2. Flare Variability Index

We have developed a flare variability index, Φ_{ug}, that is a modified version of an index originally designed to measure variability in multi-epoch and multi-band photometry (Welch & Stetson 1993; Stetson 1996). The Welch and Stetson variability index is often employed for periodic variable searches, e.g., for Cepheids and RR Lyrae stars. Our modification produces a variability index that is calculated on an epoch-by-epoch basis. The flare variability index, Φ_{ug}, is based on measuring positive flux increases in both the *u* and *g* filters, since the defining characteristic of stellar flares is the dramatic enhancement in the blue continuum emission (Moffett 1974). Note that the photometric data in the UW time-resolved database are given in magnitudes, which we convert to nanomaggies (nMgy), a linear flux density unit, via Equation (1) in Ivezić et al. (2007). One Mgy corresponds to a flux density of 3631 Jy (Oke & Gunn 1983; Finkbeiner et al. 2004; Blanton et al. 2005). With fluxes

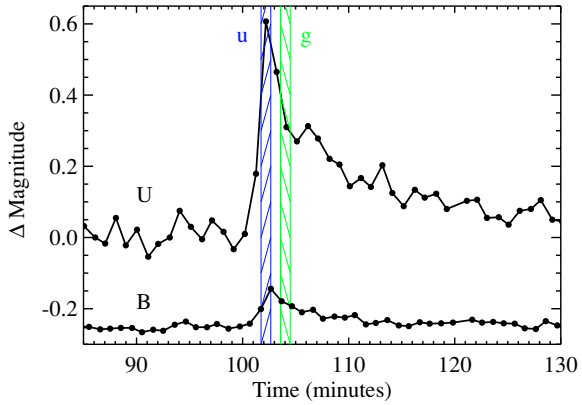

Figure 5. Example light curves in U and B of time-resolved broadband photometry during a ∼0.6 U-band peak magnitude flare (A. F. Kowalski et al., 2009, in preparation). The time sequence of the SDSS u (blue) and g (green) filters are shown as the hashed regions in the unlikely scenario that the u-band integration caught the flare exactly at the peak. The time sequence introduces uncertainty in the interpretation of the SDSS flare emission, especially for small, short-lived flares.

(A color version of this figure is available in the online journal.)

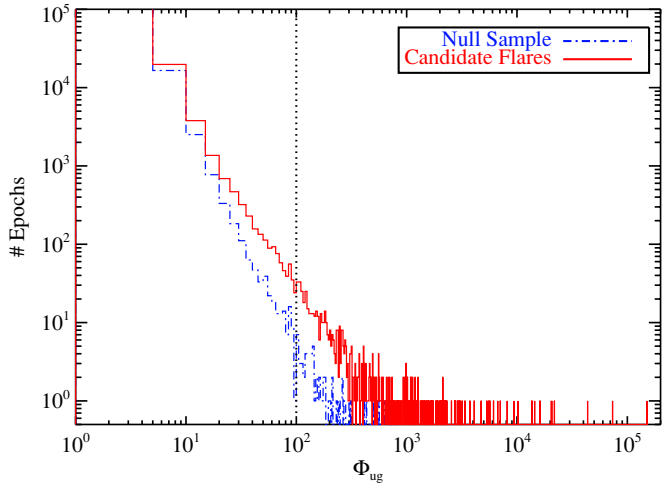

Figure 6. Distribution of the flare variability index for our candidate flare distribution (red curve; $\Phi_{ug} > 0$, $F_{u,j} - F_{u,q} > 0$, and $F_{g,j} - F_{g,q} > 0$) compared to the distribution of $\Phi_{ug} < 0$ (blue curve) shown for the same number of epochs (∼770,000). The former comprises both candidate flares and random night-to-night photometric variation, while the latter results purely from random photometric variation. The vertical line indicates the threshold value of $\Phi_{ug} = 100$ which provides <10% false discoveries, and gives 673 candidate flares (see the text).

(A color version of this figure is available in the online journal.)

expressed in nanomaggies, we quantify the increases in the u and the g fluxes at a given epoch on a given star by comparing them with the measurement errors:

$$\Phi_{ug} = \frac{(F_{u,j} - F_{u,\mathrm{quiet}})}{\sigma_{F_{u,j}}} \times \frac{(F_{g,j} - F_{g,\mathrm{quiet}})}{\sigma_{F_{g,j}}}, \qquad (1)$$

where Φ_{ug} is the flare variability index evaluated at epoch j, $F_{u,j}$ is the flux in the u filter at epoch j, $F_{u,\mathrm{quiet}}$ is the mean u flux for the star, and $\sigma_{F_{u,j}}$ is the photometric uncertainty in the u flux at epoch j; the same notation is used for the g filter quantities. The quiet flux values $F_{u,\mathrm{quiet}}$ and $F_{g,\mathrm{quiet}}$ are taken to be the weighted means of the well-measured epochs (see Section 2.1).

Flares will have positive flux deviations in both u and g,

$$F_{u,j} - F_{u,\mathrm{quiet}} > 0; \qquad F_{g,j} - F_{g,\mathrm{quiet}} > 0, \qquad (2)$$

generating a positive value of Φ_{ug}. Note that eclipses, which have negative flux deviations in both filters, also generate a positive value of Φ_{ug}, while the subset of random noise characterized by positive flux deviation in one filter, negative in the other, generates a negative value of Φ_{ug}. To insure that eclipses are not included as candidate flare events, we require that the u-band flux enhancement be positive.

3.3. Flare Candidate Selection

The quiet flux of M dwarfs in the u band is very faint, in most cases close to our apparent magnitude limit of $u = 22$. Thus, we expect that photometric variations caused by random sampling of noisy data (e.g., the significant noise apparent in the u and g light curves in Figure 4) will in some cases produce positive values of the flare variability index, and hence masquerade as flares. The false discovery rate (FDR) method of Miller et al. (2001) allows us to further limit the number of positive Φ_{ug} events that are candidate flares. The FDR analysis involves comparing a source distribution with a null distribution, and then using the null distribution to assign a probability that a given value of Φ_{ug} is drawn from the null. Figure 6 compares the candidate flare (source) distribution ($\Phi_{ug} > 0$, $F_{u,j} - F_{u,\mathrm{quiet}} > 0$, $F_{g,j} - F_{g,\mathrm{quiet}} > 0$), with the random noise (null) distribution ($\Phi_{ug} < 0$), for the same number of epochs in each distribution (∼770,000). It is clear that a significant number of the candidate flares, especially at low values of Φ_{ug}, can be attributed to random noise. FDR analysis provides a way to select a threshold Φ_{ug} value that limits the percentage of false positives. Employing the IDL routine in Appendix B of Miller et al. (2001), we determined that setting the FDR parameter, α, to 10% corresponds to $\Phi_{ug} \sim 100$ (the vertical line in Figure 6). Therefore, no more than 10% of the epochs with $\Phi_{ug} \geqslant 100$ are false positives caused by random sampling of noisy data. This returned a reasonable number (673) of candidate flare epochs for individual examination.

As shown in Figure 5 and described briefly in Section 3.1, flares with small flux enhancements typically occur over short timescales and may not be detected in both the u and g filters during the SDSS imaging cadence. An additional complication is that the SDSS u-band imaging suffers from a photometric defect known as the "red leak" caused by the u filter which allows flux with wavelength longer than 7100 Å to be partially transmitted. Due to the complexity and time dependence of this instrumental artifact, it is not corrected for in the SDSS photometry.[8] We investigated the red leak by analyzing SDSS images taken at a range of air masses. The differential refraction between the blue and red light separates the red leak photons into a faint image that is offset from the (blue, u band) stellar image at the parallactic angle and with the correct image displacement, ranging from 1.″15 to 2.″4 (Filippenko 1982). As a result, there may be various degrees of point-spread function (PSF) deblending from observation to observation depending on the seeing, air mass, and stellar and flare colors. We show examples of the red leak effect in Figure 7. In the two worst cases, we estimate that the amount of the red leak would have added ∼0.3 and 0.5 mag to the u-band measurements had they been co-aligned and therefore not deblended. Thus, we do not trust any measured u-band magnitude enhancements of 0.5 mag

[8] See http://www.sdss.org/dr7/products/catalogs/index.html for a summary description of the red leak.

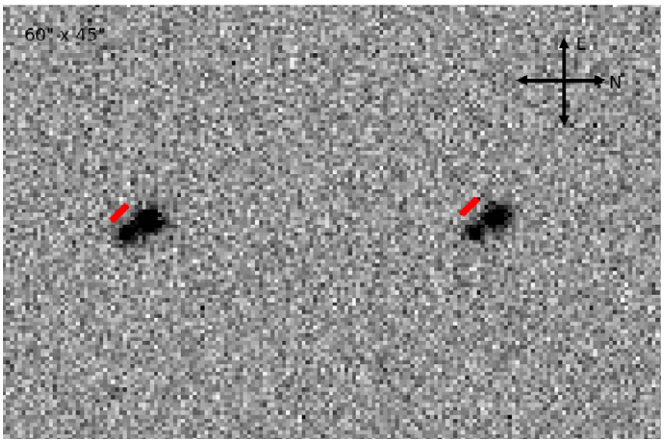

Figure 7. Example of the red leak in SDSS u-band images for two red stars (both $g - r = 1.44$) during a nonflaring epoch (run = 6590, camcol = 2, field = 218) at a high air mass of 1.64. These represent the worst cases of red leak encountered, with nearly complete separation of the red leak and true stellar images. A line at the parallactic angle with length equal to the displacement of ∼2.″3 predicted from Filippenko (1982) is overplotted in red next to each star. If all the red leak flux were added to the u flux and not deblended, the red leak would contribute approximately 0.5 mag to the photometry for each star.

(A color version of this figure is available in the online journal.)

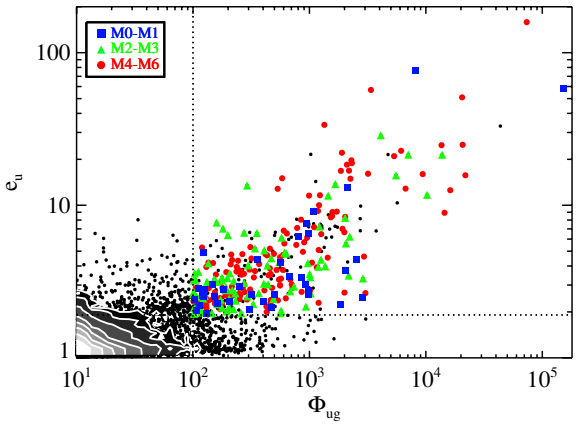

Figure 8. Flux enhancement in the u filter vs. Φ_{ug} for $\Phi_{ug} > 0$, $F_{u,j} - F_{u,q} > 0$, and $F_{g,j} - F_{g,q} > 0$. The vertical line corresponds to critical threshold $\Phi_{ug} = 100$ and the horizontal line corresponds to a Δu mag = 0.7. The 271 flaring epochs are shown as colored circles, while the observations which are cut out by flags or image inspection are left as black circles. The contours correspond to density levels of (5, 10, 25, 75, 150, 300, 600, 1200) in bins of $\Delta\Phi_{ug} = 5$, $\Delta e_u = 0.1$.

(A color version of this figure is available in the online journal.)

or less. Since, as described in Section 1, we only want to analyze bona fide flares, we adopt a conservative limiting magnitude of $\Delta u = |u_{\rm flare} - u_{\rm quiet}| \geqslant 0.7$ mag, which corresponds to almost a factor of 2 increase in the flux, as the lower limit of our flare detection capability. Requiring a correlated increase in g is an additional safeguard against erroneously selecting "flares" due to the red leak.

Flares typically show blue continuum emission with the approximate spectral shape of a 10,000 K blackbody (Hawley & Fisher 1992, see also Figure 5). This characteristic implies that the flux enhancement in u should be greater than that in g,

$$e_u = \frac{F_{u,j}}{F_{u,\rm quiet}} > \frac{F_{g,j}}{F_{g,\rm quiet}} = e_g. \quad (3)$$

All but two of the candidate flares exhibit this characteristic. The time evolution of the flares combined with the image sequencing adds ambiguity to the precise spectral shape of the flares, and so we do not exclude candidate flares that fail to exhibit this characteristic. In rare cases, observations during the rapid rise phase of the flare, if the u band was measured just as the flare started, and the g band slightly later, at the peak of the flare, might show $e_g > e_u$.

The number of candidate epochs is now small enough that each can be queried in the time-domain database to return photometry flags, as was originally done for the SDSS DR6 Stripe 82 photometry (see Section 2.1). The following flags cuts were applied in the u and g bands to eliminate observations with poorly determined photometry: SATURATED, NODEBLEND, NOPROFILE, PSF_FLUX_INTERP, BAD_COUNTS_ERROR, INTERP_CENTER, DEBLEND_NOPEAK, NOTCHECKED, MAYBE_CR, and SATURATED = 0. Note that most of the rejected epochs resulted from having NODEBLEND set, indicating that a star is seen as two fainter objects in good seeing, but a brighter object (masquerading as a flare) in poor seeing, when the two objects cannot be deblended.

The candidate flare sample has now been pared as much as possible by statistical analysis, noise requirements, and flare physics. Further analysis requires visual inspection of the data for each epoch. An image was retrieved and examined to look for artifacts such as diffraction spikes. The light curves were also examined to insure that the data are consistent with those seen from flares (e.g., Figure 4). Finally, to confirm the increases in flux indicated by the automatic SDSS PSF photometry, we identified a nonflaring epoch for each star that had a candidate flare epoch, and ran a PSF-matching and image subtraction algorithm developed for the SDSS-II Supernova Survey and the Deep Lens Transient Survey (Becker et al. 2004). During a true flare, the field stars will disappear in the subtracted images, and the flare star will show residual PSF structure in both the u and g images. For cases with unusual PSF structure or data taken with poor seeing, we calculated the aperture photometry for the flare star and compared to several other stars in the field, as the aperture photometry should be independent of the PSF shape. Only nine flare candidates were eliminated through this visual inspection, image subtraction, and aperture photometry process.

Figure 8 shows the selected flare candidate region in a plot of u-band flux enhancement versus flare variability index. Black points show all observations with $\Phi_{ug} > 0$, $F_{u,j} - F_{u,q} > 0$, $F_{g,j} - F_{g,q} > 0$. The vertical line corresponds to $\Phi_{ug} = 100$ and the horizontal line corresponds to $e_u = 1.91$ (Δu mag = 0.7). The 271 flare epochs are shown as circles, colored by most probable spectral type. To the left of our Φ_{ug} threshold, observations may have a large flux enhancement; however, they are not selected due to either a large photometric error in u or a negligible increase in g. We inspected several candidate epochs that fell just short of making our cuts, and found that the return in actual flare observations was very small compared to the increase in the number of candidate epochs resulting from weakening our criteria.

3.4. Summary of Flare Sample

Table 2 summarizes the steps we took to arrive at our final flare sample, which consists of 271 epochs (225 from the $ugriz$ sample and 46 from the ug-only sample) on 236 stars. We verified that the fraction of observations that flare for all the runs is fairly uniform, consistent with observing random stellar events and not the result of photometric artifacts on one or a few nights. There are 38 flares (38 stars) on early M0–M1 dwarfs out

Table 2
Flare Selection Criteria

Criterium	*ugriz*	*ug*	Spectroscopic (SDSS)	Justification
Clean sample	39,633 (1,987,253)	10,497 (524,981)	4005 (197,867)	M star colors, no WD-dM
$\Phi_{ug} > 0$	39,629 (1,031,706)	10,497 (272,249)	4004 (102,582)	$\Phi_{ug} < 0$ from noise in u and g
$F_{u,j} - F_{u,\mathrm{quiet}} > 0$, $F_{g,j} - F_{g,\mathrm{quiet}} > 0$	39,620 (612,728)	10,484 (158,550)	4004 (61,107)	Eliminates possible eclipses
$\Phi_{ug} \geqslant 100$	321 (463)	132 (210)	36 (51)	FDR
Δu mag $\geqslant 0.7$	243 (296)	60 (74)	29 (38)	Red leak
SDSS photometry flag cuts	201 (231)	44 (49)	··· (···)	···
Image check	195 (225)	41 (46)	23 (29)	···

Notes. The criteria for selecting flares are shown, separately for the *ugriz* sample, the *ug*-only sample and the spectroscopic sample (those stars with SDSS spectra). The number of stars is given, and the number of epochs is shown in parentheses. The final flare sample contains 236 stars with 271 flaring epochs.

of 1,783,142 epochs (35,024 stars) observed; 83 flares (79 stars) on mid M2–M3 dwarfs out of 629,170 epochs (12,986 stars) observed, and 150 flares (119 stars) on later M4–M6 dwarfs out of 99,922 epochs (2120 stars) observed. Clearly the flaring fraction is much higher on the later-type stars, both because they are more likely to be magnetically active, and because flares at the level of twice the quiescent brightness are much lower energy on fainter stars, and therefore likely to be observed more often. These results are discussed further in Section 4.1. Note that several of the redder stars flared multiple times, with the highest occurrence being five flares (and possibly several more small flares that failed to make our cuts) on an active M5 star (SDSS J025951.71+004619.1).

4. RESULTS AND DISCUSSION

4.1. The Fraction of Stars That Flare

The Stripe 82 imaging data provided observations of 2, 512, 234 epochs with reliable photometry in both the *u* and *g* bands, from which we confidently identified 271 flares. This gives an overall flaring fraction of $0.0108 \pm 0.0007\%$. In other words, about one of every 10, 000 observations in Stripe 82 of a star with the colors of an M dwarf and $u < 22$ resulted in a flare detection with $\Delta u \geqslant 0.7$ mag. Several factors enter into this determination of the flaring fraction: the stellar density distribution being sampled to an apparent magnitude limit of $u < 22$, resulting in a large number of early type M dwarfs in the sample; the fact that active stars are more likely to flare, and are more likely to be of later spectral type and therefore are being sampled over a smaller volume; and the flare detection limit of $\Delta u \geqslant 0.7$ mag which results in lower energy flares being detectable only on intrinsically fainter stars. We discuss each of these effects separately.

As expected, the stars that were known to be active, based on SDSS spectral observations showing Hα in emission, flared much more frequently. Out of 10,396 observations of known active stars, we found 29 flares, which gives a flaring fraction of $0.28 \pm 0.05\%$, ∼30 times higher than the flaring fraction for the whole sample. There were no known (from SDSS spectra) inactive stars that flared (but see Section 4.2). As far as we are aware, these are the first determinations of the flaring fraction of M dwarfs (and active M dwarfs) as a Galactic population.

Redder stars (later spectral types) also were found to flare more frequently than earlier type stars, as expected because they are more likely to be active and because lower energy flares are detectable due to their lower surface temperatures and fainter quiescent fluxes. The top left panel of Figure 9 shows the flaring fraction separated by spectral type group. The fractions differ by about an order of magnitude for each group, ranging from 2×10^{-5} for the M0–M1 stars to 1.3×10^{-4} for the M2–M3 stars to 1.50×10^{-3} for the M4–M6 stars. It is notable that the M4–M6 stars had a factor of 18 fewer observations (100,000 compared to 1.8 million) yet had nearly four times as many flares. Clearly, the later-type stars form the bulk of the flare sample.

Figure 3 shows that the total sample is sparsely populated by stars with spectral types M5 and later since they must be nearby to pass the $u < 22$ threshold. In fact, ∼96% of the observations in the M4–M6 bin are of M4 stars. If we examine the M4 and M5–M6 bins separately, the flaring fractions become $1.2 \times 10^{-3} \pm 1 \times 10^{-4}$ for M4's and $8.5 \times 10^{-3} \pm 1.5 \times 10^{-3}$ for M5–M6's, continuing the order of magnitude increase in flaring fraction toward later-types. However, the small number of stars (82), epochs (3656), and flares (31) on M5–M6 stars in the sample makes this value relatively uncertain, so we do not include it in Figure 9.

If we remove the dependence on activity by plotting the flaring fraction of only the known active stars for each spectral type group (bottom left panel of Figure 9), the fractions are significantly higher but the trend with spectral type remains. The detection limit, $\Delta u \geqslant 0.7$, may be a contributing factor to the high flare fraction on the later spectral type stars. We can investigate this effect by considering only large flares, where a large flare is defined as having a *u*-band luminosity greater than 1% of the bolometric luminosity (see Section 4.4 for details on the calculation of flare luminosities). These higher luminosity flares will be detected at all spectral types in our sample. Although there are fewer flares that are large (73), they provide a comparison of the flare fractions between early-, mid-, and late-types without a threshold bias. Figure 9 (bottom right panel) shows the fraction of flaring epochs with large flares. The flaring fraction for the later-type M dwarfs is still an order of magnitude larger than for the early-types, indicating that the detection threshold is not the main factor contributing to this result.

4.2. The Flaring of (Relatively) Inactive Stars

In the SDSS spectroscopic sample, every star that flared showed Hα emission in its quiescent spectrum. To further investigate the activity status of the stars that flared but had no SDSS spectra, we obtained follow-up spectra of 76 additional stars using the DIS spectrograph on the ARC 3.5 m telescope (see Section 2.3). These spectra were spectral typed and had Hα emission measured using the Hammer analysis software (Covey et al. 2007). The results are given in Table 3. Seven stars show no

Table 3
APO 3.5 m DIS (R300) Spectral Sample

SDSS ID	Spectral Type	Hα EW (Å)	Notes	Activity	Dates
J203940.38+001326.7	M1	1.4	···	y	080825
J204133.37-001958.5	M5	4.7	···	y	080919
J204144.10+004048.2	M4, M4	0.4, 1.5	···	n, n	081107, 080919
J204452.77+010546.9	M1, M2	0.3, 0.9	···	var	081107, 080919
J204725.80+004128.0	M2	3.3	···	y	080919
J204728.12+002206.6	M4	8.9	···	y	080919
J205020.88-010839.9	M3	3.5	···	y	080919
J205300.05-003821.8	M3	3.8	···	y	080919
J205632.51+001413.5	M1	2.2	···	y	080919
J210012.57-005326.0	M5	3.8	···	y	080919
J210023.79-005830.1	M0	0.8	···	w	080919
J210034.02-005814.6	M6	6.3	···	y	080919
J210343.88+000303.1	M3	7.0	···	y	080919
J211110.85+005027.1	M4	4.5	···	y	080919
J211138.04+002137.2	M4	5.9	···	y	080919
J211311.65-002503.2	M4	4.1	···	y	080919
J211414.08-005534.7	M5	5.0	···	y	080919
J211454.52-000215.3	M4	5.3	···	y	081107
J211827.00+000248.5	M2, M0, M1	1.6, 1.4, 0.8	···	y, y, w	081107, 080825, 081214
J212133.89-011137.4	M4	5.5	···	y	080919
J212749.79+002607.2	M3	2.9	···	y	081107
J213112.08-002154.0	M4	4.5	···	y	081107
J213206.27+004026.9	M5	7.8	···	y	080919
J213517.94-005725.1	M1	1.6	···	y	080919
J214029.24+003320.6	M3	1.0	···	w	080919
J214124.51-002220.5	M4	2.0	···	y	081214
J214226.15+010542.3	M1	0.5	···	w	080919
J214245.57-005436.7	M1	1.2	···	y	080919
J214751.69-003237.4	M4	3.9	···	y	080919
J215430.88+002117.0	M4	3.3	···	y	080919
J220548.89-000352.5	M1, M1	0.0, 0.2	···	n, n	080825, 080919
J220920.29-005738.8	M2	2.4	···	y	081214
J221726.10+003052.2	M3	2.9	···	y	081013
J222012.89-003429.0	M1	1.3	···	y	080825
J222552.54+000251.6	M4	4.1	···	y	080919
J223711.01+005306.5	M2	2.6	···	y	080919
J223731.35+005425.6	M5	3.9	···	y	081013
J225641.87+011050.9	M5	2.8	···	y	080825
J230001.05+010454.1	M5	5.6	···	y	081107
J230314.24-003110.7	M2	2.7	···	y	080825
J231109.45+002515.4	M3	4.2	···	y	081107
J231810.79-004512.3	M2	3.4	···	y	080825
J232516.19-001600.9	M2	1.8	···	y	080825
J233810.08-004450.3	M4	4.3	···	y	080825
J233952.93-001005.3	M5	5.8	···	y	080825
J234612.94+002507.3	M1	0.0	···	n	081107
J004145.91-002832.7	M5	6.0	···	y	080825
J005847.77+011015.5	M4	4.5	···	y	080825
J010052.58+010233.1	M0	−0.2	···	n	081107
J011745.28+005929.4	M1	1.8	···	y	081013
J012531.29-005359.0	M3	2.7	···	y	080825
J013851.46-001621.7	M6	12.0	···	y	081013
J020056.76+004149.1	M4	9.2	···	y	081013
J020327.92-000442.1	M3	3.1	···	y	081013
J022112.48+003225.7	M4,M3	0.7,0.8	···	n,n	080825, 080919
J022214.35-003217.5	M2, M2	0.7, 0.6	···	w, w	081013, 081124
J023452.37-010031.4	M3	3.3	···	y	081107
J023538.57-000422.2	M4	6.0	···	y	081107
J023547.98-005822.4	M3	2.1	···	y	081107
J023550.72+010136.8	M3	2.3	···	y	081124
J024554.14-010445.1	M3	6.0	···	y	081124
J025747.56+004731.2	M4	3.8	···	y	081124
J032605.67-002402.6	M0	2.0	···	y	081124
J033017.55+005359.4	K7	−0.5	···	n	081124
J033734.14-011104.5	M2, M3	−0.6, 0.0	···	n, n	081013, 081124

Table 3
(Continued)

SDSS ID	Spectral Type	Hα EW (Å)	Notes	Activity	Dates
J033735.25+005859.7	M2	2.4	...	y	081124
J205059.98+005136.4	M4	2.4	*ug*-only	y	080919
J205257.83-000335.9	M3	3.3	*ug*-only	y	080919
J215455.18+011414.5	M0	6.0	*ug*-only	y	081214
J215517.42-004547.9	M5	11.6	*ug*-only	y	081214
J221712.10-000815.4	M0	−0.4	*ug*-only	n	081214
J001208.37+002559.1	M4	5.7	*ug*-only	y	081214
J005903.60-011331.1	M2	2.6	*ug*-only	y	081214
J011307.16-002326.1	M3	3.4	*ug*-only	y	081214
J012904.68+003058.4	M5	2.3	*ug*-only	y	081214
J020911.90+004432.4	M1	1.2	*ug*-only	y	081214

Notes. y, active; w, weakly active; n, inactive; var, variable. Activity status was determined using the criteria in West et al. (2004, 2008) and types were determined automatically with the Hammer facility (Covey et al. 2007). The automatically assigned activity status and type were adjusted by eye as needed, and EW's were recalculated accounting for the radial velocity shift. Errors in the EW are typically ∼0.2 Å, and were calculated using Equation (A10) in Chalabaev & Maillard (1983).

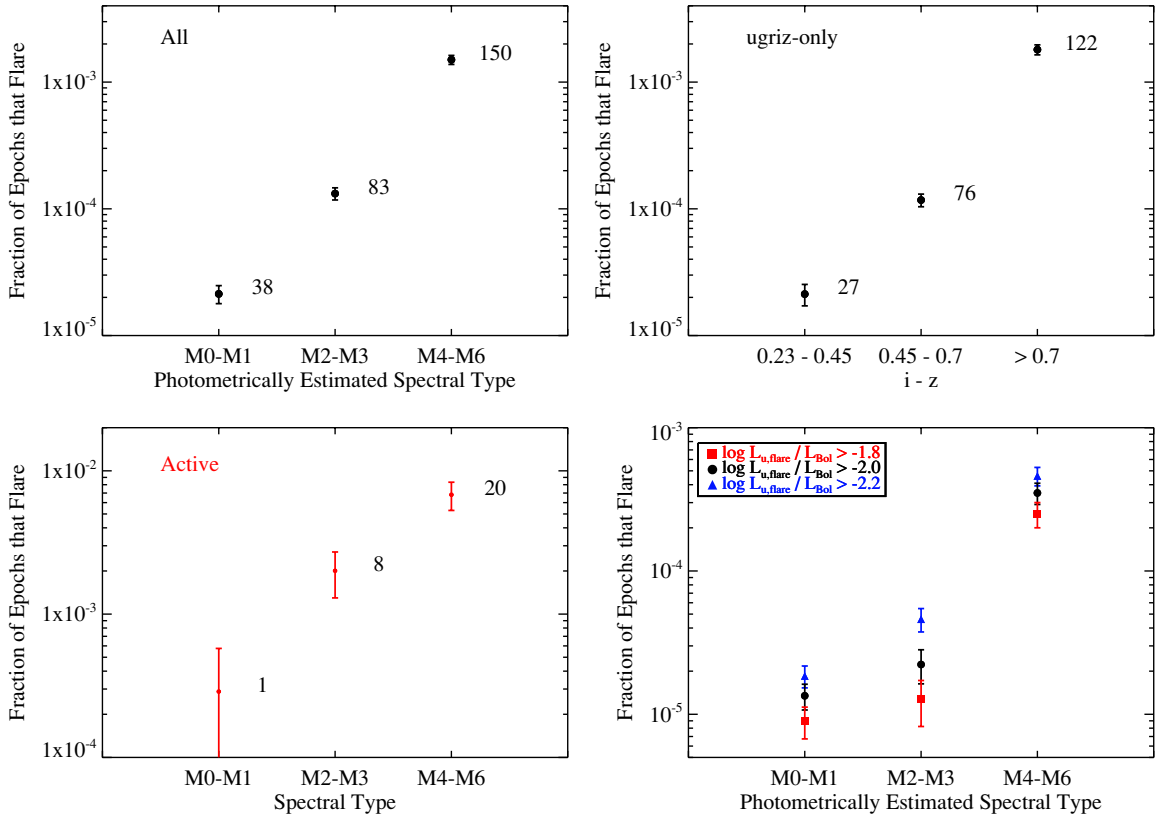

Figure 9. Top, left: the flaring fraction for the entire sample, binned according to the photometrically estimated spectral type. The numbers indicate the number of flares in each spectral type bin. Top, right: the flaring fraction for the *ugriz*-only sample using $i-z$ color bins, showing that using either color or spectral type isolates the same groups of stars. Bottom, left: the flaring fraction for the active stars with SDSS spectra only, binned according to the spectral type determined from each spectrum. The flaring fractions for the active stars are significantly larger than for the entire sample. Bottom, right: the fraction of epochs that are large flares, using several values of $L_{u,\mathrm{flare}}/L_{\mathrm{Bol}}$ to define a large flare. Although it is easier to see low-luminosity flares in the late-type dwarfs (contrast effect), the high-luminosity flares can be detected at all spectral types. The number of flares in the (early, mid, late) type bins are (33, 29, 46), (24, 14, 35), and (16, 8, 25) for the triangles, circles, and squares, respectively.

(A color version of this figure is available in the online journal.)

evidence of Hα emission. One star, SDSS J022112.48+003225.7, has an ambiguous signature near 6563 Å, but this feature may be a blend of Hα and a TiO band known to exist in inactive M4 stars at this wavelength. Without higher resolution spectra, we group this star among the inactive stars. Another star, SDSS J204452.77 + 010546.9, exhibited variable Hα emission between *no* activity and *weak* activity on two different epochs (UT081107 and UT080919). Perhaps we happened to catch the UT080919 spectrum at the tail end of a flare; however, an analysis of the low-signal B400 spectra (3400 Å–5500 Å) showed no significant change in color between the two epochs, indicating that the observation would have likely not met our flaring criteria. We classify this object as *variable*, a known trait of active M dwarfs (Gizis et al. 2002).

Of the eight likely inactive stars, four were observed on two separate nights to confirm the lack of emission. The spectral types for the eight stars show no obvious trend toward early- or late-type (*Hammer type* (photometric type): *K7* (M0), *M0* (M0), *M0* (M0), *M1* (M0), *M1* (M0), *M3* (M3), *M4* (M4), *M4* (M3)) but the numbers are too small to draw any conclusion about the spectral type distribution of inactive stars that flare. Though formally classified as inactive, these stars may be part of a group of weakly active M dwarfs which show Ca II H and K emission but Hα absorption (Walkowicz & Hawley 2009). Certainly, the fact that they flared is a strong indication that they possess surface magnetic fields.

From our combined spectroscopic sample (SDSS + DIS) of (23+76 = 99) stars, with eight being classified as inactive due to lack of Hα emission, we derive a preliminary fraction of flaring stars that are inactive to be ~8% (the binomial errors on this percentage are 1.9%, +3.6%). In other words, out of every 12 stars that flare in the SDSS Stripe 82 region, one of them might be inactive. This is an important value to determine for modeling the rate of flares in the Galaxy, since as noted in Section 2.2, most M dwarfs are inactive, especially at early–mid spectral types.

4.3. The Flaring Fraction Versus Distance from the Galactic Plane

As a result of dynamical encounters, stars can move farther from the Galactic plane as they age. The mean stellar age thus tends to increase as a function of vertical distance $|Z|$ from the plane. Therefore, other stellar properties that change with the lifetime of the star should also change with $|Z|$ distance. The fraction of active stars in the SDSS DR5 sample was found to decrease with $|Z|$ for each M spectral type (West et al. 2008), indicating that magnetic activity depends on age. Many other studies have linked chromospheric activity to stellar age (Wilson & Woolley 1970; Wielen 1977; Giampapa & Liebert 1986; Soderblom et al. 1991; Hawley et al. 1996, 1999, 2000).

Figure 10 shows the dependence of the flaring fraction on vertical distance (age) for our three spectral type groups. Computing the *fraction* of epochs that flare effectively normalizes by the local stellar density and accounts for varying incompleteness in different distance bins. Distances were estimated using an $r-z$ photometric parallax relation (Bochanski 2008) for stars in the $ugriz$ sample and a $g-K$ photometric parallax relation (Covey et al. 2008a) for stars in the ug-only sample. As discussed previously, to obtain accurate estimates for the distances we applied interstellar extinction corrections to the $r-z$ and $g-K$ colors before using the photometric parallax relations. The Sun was taken to be 15 pc above the Galactic plane (Cohen 1995; Ng et al. 1997; Binney et al. 1997). The fraction of epochs where flares were detected decreases sharply with $|Z|$ distance for all three spectral type groups. This is expected because of the age dependence of (quiescent) magnetic activity, and the strong correlation between active stars and stars that flare. As mentioned in Section 2.2, the volume over which the stars are measured differs markedly for the different groups. The later-type group is sampled only at close distances, while the mid- and early-type groups are sampled progressively farther from the plane. The cumulative distributions for the flaring epochs (asterisks), active epochs (triangles), and all epochs (open squares) are given in the bottom panel of Figure 10 and show the combined effects of age, spectral type, and stellar density distribution in an apparent-magnitude limited sample. More than half the stars in the sample are at a distance greater than 300 pc from the plane,

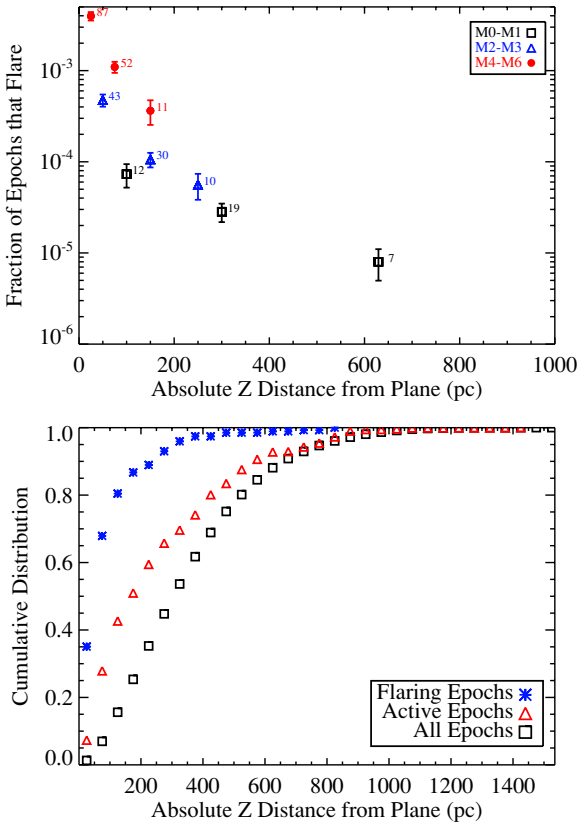

Figure 10. Top: the flaring fraction for different spectral type bins as a function of $|Z|$ distance from the plane. The M0–M1 stars are plotted in bins of 0–200 pc, 200–400 pc, and 400–900 pc; M2–M3 stars are plotted in bins of 0–100 pc, 100–200 pc, and 200–300 pc; M4–M6 stars are plotted in bins of 0–50 pc, 50–100 pc, and 100–200 pc. Note the differences in volume sampled for the different spectral types (due to the u apparent magnitude limit). Also, note the sharp decrease in flaring fraction as older populations are sampled farther from the Galactic plane. Bottom: the cumulative distributions of $|Z|$ distance for all epochs (black squares), active epochs (red triangles), and flare epochs (blue asterisks), in bins of 50 pc. The most distant flare occurs on a star that is ~850 pc below the plane, while the most distant star is located at ~1500 pc below the plane.

(A color version of this figure is available in the online journal.)

but less than 10% of the flares occur on stars that far away. Since the thin disk outnumbers the thick disk until ~1 kpc (Jurić et al. 2008), it is likely that these distant stars that flare still belong to the thin disk population. Although 70% of the active epochs are within 300 pc, a third of the active stars are early-type stars which do not contribute significantly to the flaring population. For these reasons and because of higher quality photometry for stars with $u < 21$, the nearby late-type, active stars clearly make the largest contribution to the flaring fraction in this sample.

The flaring fraction shows a larger decrease with increasing $|Z|$ distance than the active fraction from West et al. (2008), especially for the M4–M6 bin. We find that an additional factor contributing to the trends seen in Figure 10 is a bias toward higher luminosity flares on more distant stars. M dwarfs are known to exhibit a large spread in $u-g$ color (Covey et al. 2008a). For a given spectral type, we find a large spread in u-band quiescent luminosity (see Section 4.4 for details on the calculation of flare luminosities). For example, the M4's in this sample have an average u-band luminosity during quiescence of $\sim 4 \times 10^{28}$ erg s^{-1} with a spread of $\sim 2 \times 10^{28}$ erg s^{-1}. For distances >200 pc, most M4s become too faint in the u band to be included in our sample.

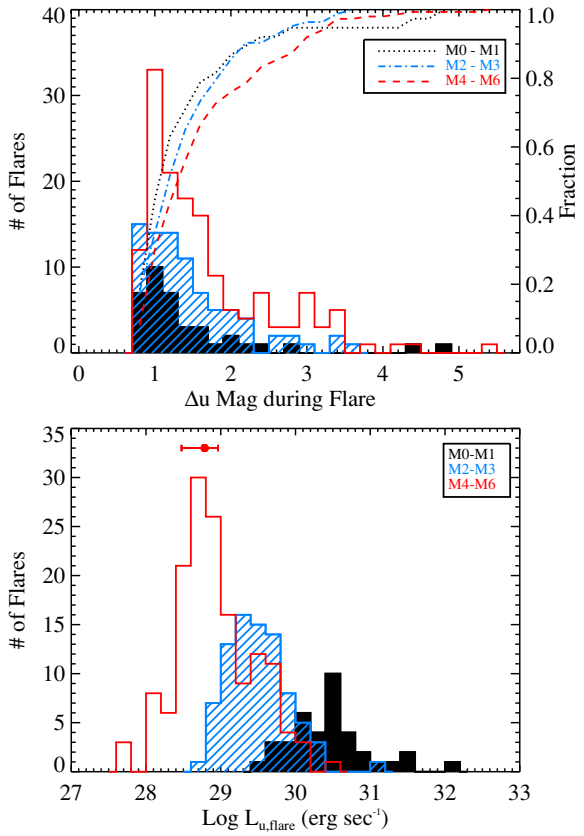

Figure 11. Top: the distribution of *u*-magnitude enhancements during flares. The dotted lines show the cumulative distributions. Later-type (lower mass) stars have the most detected flares and generate very large magnitude enhancements (due to their smaller quiescent luminosity). When converted to luminosities (bottom), the flares on the higher mass stars are the most luminous. Both of these results are consistent with previous flare observations. The errors in luminosities are ∼50%, and we show a typical error bar.

(A color version of this figure is available in the online journal.)

At these large distances, only the M4s which are intrinsically bright are included (i.e., there is a Malmquist bias due to our apparent magnitude selected sample). Therefore, a flare with $\Delta u = 0.7$ magnitudes on an intrinsically bright M4 has a larger *u*-band luminosity than a flare with the same apparent enhancement on an intrinsically fainter M4. More luminous flares (or more luminous stages of flares) occur less frequently (Lacy et al. 1976), which generates a bias in our sample toward smaller flare fractions at greater distances. A useful future study would be to examine flare rates for a flare-luminosity limited sample.

We also note that Welsh et al. (2007) found that most of the M dwarf flares detected in NUV Galex observations (1750 Å–2750 Å) occur on stars within 300 pc of the plane; the flare flux in the NUV and *u* bands is thought to come from the same (or similar) emission mechanism, so it is expected that flare detections in these wavelength regimes should trace one another through the Galaxy.

4.4. Flare Magnitudes and Luminosities

Figure 11, top, shows the distribution of flare magnitude (Δu) for the three spectral type groups. The later-type stars generally show larger magnitude increases, due to their lower quiescent luminosity. In other words, it is much easier to see an energetically small flare on a star that is intrinsically fainter. Since the flare detection limit was chosen to be $\Delta u \geqslant 0.7$ mag on all stars, this corresponds to a lower luminosity flare on the intrinsically fainter star. This relationship is consistent with previous flare studies (e.g., Moffett 1974; Rockenfeller et al. 2006). Figure 11 shows empirically which stars are likely to be observed with large magnitude increases, which is the metric of interest for time-domain surveys searching for transient brightness variations.

To obtain flare luminosities, the quiescent stellar *u*-band flux was subtracted from each flare observation, and the fluxes (which are per Hz) were converted to luminosities using the distance to each star (see Section 4.3) and the nominal *u* bandwidth (FWHM 1.33×10^{14} Hz, or roughly 600 Å). Again, we use extincted-corrected magnitudes for the luminosity calculations. The flare luminosity distributions by spectral type are illustrated in the bottom panel of Figure 11. We calculate the errors on the luminosities to be ∼50%, which is dominated by the error in the photometric distance determination and includes the uncertainty in the amount of red leak flux (up to 30%) contained in the measured quiet *u* magnitude. Systematic errors in the luminosity calculation are introduced since we assume full line-of-sight corrections for interstellar extinction. As mentioned in Section 2.2, corrections effectively increase the distances, thereby increasing the luminosities by ∼10%–70%.

In Figure 11, the low-luminosity cutoff of each distribution represents the detection limit of $\Delta u = 0.7$ mag, which corresponds to nearly an order of magnitude difference in luminosity for each group ($\log L \sim 28.0$ for M4–6, ∼28.7 for M2–3, ∼29.5 for M0–1). Although the flare magnitude enhancements on the earlier-type stars are smaller (as shown in the top panel), their derived luminosities are generally larger than the flares on the later-type stars. This is consistent with the findings of Lacy et al. (1976) and Pettersen (1988) that the average rate of energy loss in the *U* band during flares increases as a function of stellar bolometric luminosity. For example, if we compare the two largest *u*-magnitude enhancements in the SDSS flares, the $\Delta u = 4.7$ flare on a M1 star gives a luminosity of 1.3×10^{32} erg s^{-1} while the $\Delta u = 5.5$ flare on a M6 star gives a luminosity of only 1.7×10^{29} erg s^{-1}. However, we emphasize that our derived flare luminosity is sampled at a random time during the flare and there is no way to determine whether the emission occurred during the rise, peak, or decay phase so it is not strictly comparable to the average energy. It is interesting that we do not observe very high luminosity ($>10^{30}$ erg s^{-1}) flares on the very red stars. This is likely due to two factors: they are quite rare on the relatively low (quiescent) luminosity stars; and the number of epochs that SDSS observed on the later-type stars is much smaller than on the earlier-type stars since the latter comprise a much larger fraction of the sample. When we compare the flare luminosity to the bolometric luminosity of the stars (Reid & Hawley 2005), we find a few flares that emit as much as ∼1%–10% of the bolometric luminosity in the *u* band, on stars of both early and late spectral types. Pettersen (1988) had determined a limit of 10^{-4} for the average L_U/L_{bol}; however, our values may represent instantaneous measurements of more luminous stages during flares.

With a common flare detection threshold ($\Delta u = 0.7$ mag) for all spectral types, the late-type stars emit less luminous, yet many more, flares. However, we find that the *total flare energy* emitted on early-, mid-, and late-type stars is approximately equal for equal observing times. For example, the peak luminosities of Figure 11 occur at $\log L \sim 30.5$, 29.3, and 28.7 erg s^{-1}, a ratio of ∼60:4:1 for early-, mid-, and late-types,

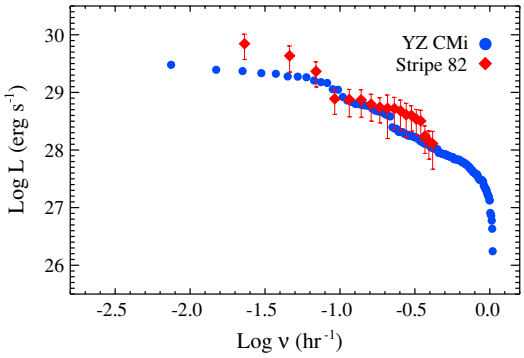

Figure 12. Flaring frequency for active M4–M5 stars from Stripe 82 compared to the average *U*-band flare frequency of the very active, nearby dM4.5e star, YZ CMi (Lacy et al. 1976). The good agreement between the two distributions demonstrates that flaring frequencies obtained from observing a large number of stars at a low cadence is consistent with observing a single flare star continuously. The SDSS Stripe 82 distribution contains 18 flares.

(A color version of this figure is available in the online journal.)

respectively. When we sum the luminosities, multiply by the filter integration time, and scale to the same total number of observations (Section 3.4), the total flare energies occur in the ratio ∼0.7:0.3:1. Apparently, the larger flare rate of the late-types approximately makes up for the lower energy output per flare, suggesting that early- and late-type stars, summed over a range of quiescent activity levels and stellar ages, may possess similar amounts of total stored magnetic energy that is eventually released as flares, but that this flare energy is released at different rates on stars of different masses. Further study of a sample including smaller flares is needed to confirm this preliminary result.

4.5. Flaring Frequency

A classic study of flare frequency for a handful of nearby, very active M dwarfs was carried out by Lacy et al. (1976). They used a monumental collection of continuous photometric monitoring data (Moffett 1974), which provided information throughout the time evolution of each flare. An average luminosity for each flare may be calculated by dividing the reported total *U*-band energy of the flare by its duration. In Figure 12, we compare the luminosities of the SDSS flares (sampled at a random time during the flare) to the average flare luminosities of the Moffett flares for the dM4.5e star YZ CMi. In order to estimate the frequency with which a flare of a particular luminosity (or greater) was seen, we used the total *u*-band observing time for active stars with SDSS spectra and spectral types of M4 or M5 (43.335 hr), and obtained a cumulative distribution of flare luminosities. As shown in Figure 12, our derived flaring frequency from the SDSS data is remarkably consistent with the flaring frequency of YZ CMi, following a power-law form with more luminous flares occurring less frequently.

4.6. Spatial Flare Rate in Stripe 82

A number of interest to characterize transient events in large sky surveys is the spatial flare rate, the number of flares per hour per square degree. Of course this rate will vary depending on which area of the sky is being observed (e.g., with Galactic latitude). For the Stripe 82 data, which span $l = (45^\circ$ to $191^\circ)$; $b = (-23^\circ$ to $-64^\circ)$ the rate can be empirically calculated by taking the number of observed flares (271), and dividing by the spatial extent of the Stripe 82 time-domain database (279.7 deg^2) and the average observing time (50 epochs × 54 s per epoch = 2700 s). This gives a rate of 1.3 flares hr^{-1} deg^{-2} with a *u* mag increase of at least 0.7 mag.

Table 4
Spatial Flare Rates

Spatial Division	Mean # Flares hr^{-1} deg^{-2}	Flaring Fraction
$23^\circ < \|b\| < 45^\circ$	2.0	1.38×10^{-4}
$45^\circ < \|b\| < 55^\circ$	0.9	9.9×10^{-5}
$55^\circ < \|b\| < 64^\circ$	0.7	8.0×10^{-5}
$45^\circ < l < 90^\circ$	1.5	1.11×10^{-4}
$90^\circ < l < 135^\circ$	0.7	8.3×10^{-5}
$135^\circ < l < 191^\circ$	0.9	1.16×10^{-4}

Notes. We present the raw spatial rate (mean number of flares hr^{-1} deg^{-2}) and the flaring fraction for different ranges of Galactic latitude and longitude. When calculating the raw spatial rate, we only consider the 1 × 1 deg^2 bins with at least 50% SDSS coverage.

The derived spatial flare rate is a lower limit to the intrinsic flare rate because we have an inefficiency, ϵ, for detecting flares. Major contributions to ϵ are varying contrast levels for the different spectral types, the fact that not all flares produce an increase in the *u* and *g* bands (e.g., flares that begin after the *u* but before the *g* observation), our limit of 10% false positives by using a Φ_{ug} threshold of 100, and our strict $u < 22$ mag cutoff. As noted explicitly, we intentionally adopted a conservative $\Delta u = 0.7$ mag limit for flare detection, so our spatial flare rate is only representative of relatively bright flares.

We calculated the number of flares divided by the average observing time per star (∼2700 s) for every square degree (in R.A. and decl.) in Stripe 82 to investigate how the number of flares hr^{-1} deg^{-2} varies with the line of sight through the Galaxy. We find a maximum flare rate of 8 flares hr^{-1} deg^{-2} occurring closer to the plane ($l \sim 56^\circ, b \sim -38^\circ$) where the density of stars is higher (∼240 stars deg^{-2} with $u < 22$ compared to the average for Stripe 82, ∼180 stars deg^{-2} with $u < 22$) and where a higher fraction of stars are active (since they are closer to the plane and therefore likely to be younger).

To illustrate how the spatial flare rate varies with Galactic latitude and longitude, we calculated the average flare rate for three latitude regions and three longitude regions.[9] Our results are presented in Table 4. This raw spatial flare rate decreases with increasing Galactic latitude, as expected due to the decreasing stellar density farther from the plane. To account for stellar density, we divided by the number of total epochs in each region and present the flaring fraction as a function of Galactic latitude and longitude in Figure 13. There is no obvious trend with longitude; however, the flaring fraction generally decreases with increasing latitude, probably because lines of sight at higher latitude include a smaller fraction of stars at small $|Z|$ distance (see Section 4.3).

Finally, the empirical flare rate for all M dwarfs would also include the flares occurring on the M dwarf–white dwarf binary systems that we excluded in step 8 of Section 2.1. We have searched those light curves and find six events that would satisfy our flare criteria. This has a negligible effect on the overall flare rate.

[9] When binning Stripe 82 into (l, b), we divided the flare rate in each 1 deg × 1 deg square by $\cos(b)$ in order to correct for the changing area due to converging lines of longitude. To compensate for incomplete coverage at the edges of Stripe 82, we also divide by the fraction of each 1 deg × 1 deg bin that was scanned by Stripe 82, and we consider only bins that have >50% coverage.

Table 5
Flare Rate Model Parameters

Spectral Subtype Bin	s	$f_{\rm active}$	$f_{a,\rm flare}$	$f_{\rm inactive}$	ν	Limiting log L_U	Predicted # Flares[a]	Observed # Flares
M0–M1	35,000	0.03	1.0	0.97	0.02	29.5	20–66	38
M2–M3	13,000	0.06	1.0	0.94	0.1	28.7	68–150	83
M4–M6	2100	0.30	1.0	0.70	0.4	28.0	193–233	150

Notes. We present the measured and derived values for the flare rate model given by Equation (4) in Section 4.6.1.
[a] We adopt 1% and 10% for $f_{i,\rm flare}$, the fraction of inactive stars that are capable of flaring, which give a range of values for the predicted number of flares.

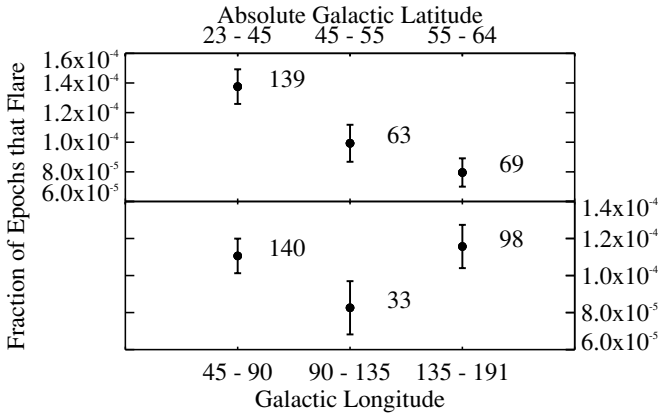

Figure 13. Flaring fraction for three divisions of Galactic latitude (top) and longitude (bottom). The flaring fraction decreases for lines of sight with larger Galactic latitude, probably because a smaller fraction of the sample is close to the Galactic plane (and therefore likely to be younger and magnetically active). There is no obvious trend with Galactic longitude. Note that the flaring fraction is a normalized quantity, so number density variations have been removed.

4.6.1. Comparison to Simple Model Prediction

For comparison, we can also estimate the flare rate from our knowledge of the spatial density of M dwarfs in Stripe 82 (Figure 3), the fraction of active stars at each spectral type (Figure 3), the relative flare rates for active and inactive stars (Sections 4.1 and 4.2), and the flare frequency distributions for stars of different spectral types (Lacy et al. 1976). This simple model calculation gives a prediction of the spatial flare rate we should observe in Stripe 82.

We consider the same spectral type ranges, and the values measured or derived previously to form the general equation:

$$\#\ \text{flares} = s \times (f_{\rm active} \times f_{a,\rm flare} + f_{\rm inactive} \times f_{i,\rm flare}) \times \nu \times t, \quad (4)$$

where s is the number of stars, $f_{\rm active}$ is the fraction of stars that are active, $f_{a,\rm flare}$ is the fraction of active stars that flare, $f_{\rm inactive}$ is the fraction of stars that are inactive, $f_{i,\rm flare}$ is the fraction of inactive stars that flare, ν is the number of flares hr^{-1} above a limiting luminosity, and t is the observing time per star. A very uncertain parameter is $f_{i,\rm flare}$, and we calculate the predicted number of flares adopting both 1% and 10%.[10] We list the measured and derived values for Equation (4) in Table 5.

In Section 3.4, we found that the number of confirmed (observed) flares was 38 for M0–M1 (compare to 20–66 predicted); 83 for M2–M3 (compare to 68–150 predicted); and 150 for M4–M6 (193–233 predicted). In all cases, the predicted values are reasonably close to the observed number of flares. Given the crude estimates in our predictions, this agreement is encouraging, indicating that our method for finding flares in the low-cadence SDSS photometric data is apparently reliable.

There are also several places where the predictions can be improved. Two very poorly determined parameters are the fraction of inactive stars that flare and the flaring frequency, ν_i, of inactive stars that flare (here taken to be the same as the flaring frequency, ν, of active stars of the same spectral type). We have an ongoing program to investigate the flaring rates of inactive stars through continuous monitoring observations (E. J. Hilton et al., 2009, in preparation).

Furthermore, our estimates for ν are taken from YZ CMi, a star with a well-determined but likely higher than average flare frequency distribution (Lacy et al. 1976). Therefore, it is not surprising that our predicted number of flares for this bin exceeds the observed number. Even if we set $\nu_i = 0$ flares hr^{-1}, 189 flares are predicted. If YZ CMi accurately represents the flaring frequency for active M4–M6 stars, we estimate our inefficiency, ϵ, for detecting flares above $\Delta u \geqslant 0.7$ mag on M4–M6 stars to be >20%, assuming that all the other parameters are correct. Alternatively, if instead we use a slightly lower flaring frequency for all M4–M6 stars, $\nu = 0.3$ flares hr^{-1}, we predict 145–175 flares, which is consistent with the observed value.

We also note that the active fraction of M4 stars found here (30%) is considerably lower than the active fraction found from the full DR5 sample (50%; West et al. 2008). DR5 is dominated by stars in the northern Galactic cap, with most observations obtained looking out of the Galactic disk. In contrast, Stripe 82 is observed through the disk, looking toward the southern Galactic cap. The difference in active fraction between the north and south is intriguing but unexplained. We are pursuing an additional study of the change in active fraction with galactic latitude.

Several regions in Stripe 82 have moderately high extinction (>0.5 mag in the g band), and we examined the possibility that the spatial flare rate is correlated with star-forming regions and therefore contaminated by accretion events. We compared the composite Hα map from Finkbeiner (2003) to the spatial distribution of stars that flare and note an absence of any conspicuous clustering of flare stars near Hα regions. The star-forming regions MBM 18/MBM 19, found at R.A. > 55°, coincide with the areas of greatest extinction in Stripe 82 and are suspected sites of low-mass star formation (McGehee 2008). None of the 11 flare stars with R.A. > 55° have spectra to examine for accretion features. Of the stars that do have spectra, none have especially high equivalent widths characteristic of accretors.

5. CONCLUSIONS

We used the multi-epoch $ugriz$ photometry of the SDSS Stripe 82 to characterize the M dwarf flaring properties as a

[10] In Section 4.2, we found that ~8% of the flare stars are inactive. Although this is not strictly the same as $f_{i,\rm flare}$, which is the fraction of inactive stars that flare, the 8% value made the adopted range of 1%–10% seem reasonable.

function of spectral type, level of magnetic activity, distance from the Galactic plane, and line of sight through the Galaxy. In contrast to studying flare rates on a few individual nearby stars via continuous monitoring, we quantify the flaring properties of *populations* of M dwarfs using low-cadence observations. We search for a flare signature on an epoch-by-epoch basis over millions of observations and employ the FDR algorithm to limit the number of false positives. We find 271 flares among ∼2.5 million observations. The fraction of epochs that flare increases by nearly an order of magnitude for each subsequently redder M dwarf color bin. We attribute this trend to there being better "flare visibility" and an increasing fraction of magnetically active stars in the redder bins.

We find a strong correlation between stars that have flares and stars that have Hα in emission during quiescence. For the sample as a whole, one out of 10,000 observations shows a flare, but ∼30 out of 10,000 epochs observed on active stars show flares. This finding is consistent with a simple physical picture connecting magnetic activity to flaring: surface magnetic loops (the source of the persistent Hα emission line) reconnect and accelerate charged particles, which then deliver energy to the lower atmosphere and produce the optical flare emission. However, the detailed physics of how such large energies in the u band are generated remains a mystery. Unfortunately, the time difference between the u and g filters adds ambiguity to the interpretation of the flare emission spectrum and prevents us from constraining the broadband spectral shape of flares with these data.

Our total sample is dominated by inactive (no Hα emission) M dwarfs, and we find only eight flaring stars that are classified as inactive. Inactive stars may have a much smaller filling factor of magnetic loops such that they do not show quiescent activity but still have a (small) chance of producing flares. Continuous monitoring of inactive M dwarfs is needed to more accurately quantify the flaring rates and properties of these stars.

The amplitudes and luminosities of the SDSS flares are consistent with previous observations. Most flares (80%) have amplitudes less than 2 mag in u, which is not surprising since random imaging is most likely to catch a flare during its more extended, smaller-amplitude decay phase. Both early- and late-type stars exhibit u-band magnitude enhancements as high as $\Delta u \sim 5$; however, the actual luminosity for a given magnitude enhancement is dependent on the intrinsic shape of the underlying stellar spectrum. Very large luminosity flares are not seen on the reddest of stars, which may be a combination of a real physical effect and a result simply from there not being as many observations of very red stars in the sample. The most luminous flares in the sample emitted ∼10% of the stellar bolometric luminosity at the time they were sampled.

The flaring fraction is found to strongly decrease with increasing $|Z|$ distance for all spectral types, as expected, due to a smaller active fraction and a Malmquist bias at greater distances. Our best estimate of the lower limit on the flaring rate (averaged over Stripe 82) for flares with $\Delta u \geqslant 0.7$ on stars with $u < 22$ is 1.3 flares hr^{-1} deg^{-2}, and the larger spatial flare rates and fractions are typically found along lines of sight at lower Galactic latitude in Stripe 82. Future time-domain surveys, such as LSST, will be able to probe to a much larger distance from the plane; however, we predict that the spatial flare rate for flares of $\Delta u \geqslant 0.7$ mag on stars from M0 to M4 will not increase appreciably for intermediate to high Galactic latitudes due to our observed $|Z|$ distance–flaring relation. For lines of sight through the Galactic plane, there is likely to be a significant increase in the observed flare rate. Since the u band will be observed only infrequently with LSST, the g and r bands will be the most useful to identify flaring epochs. We find that ∼95% of the flares have g magnitude enhancements of <1 mag. However, due to the higher precision (∼5 mmag at the bright end; Ivezić et al. 2008) of LSST, a larger number of small amplitude flares will be observed. For these reasons, flares will likely form a *larger* population of transients in LSST compared to SDSS, which was limited by the photometric uncertainties in the u band. Since the SDSS flares were selected from the u and g bands, the properties of these flares in the other bands could be applied to candidate flares in future surveys which do not use the u band.

The authors thank the referee, Terry Oswalt, whose comments greatly improved this paper. We also thank Chris Miller and Andy Connolly for their insightful discussions regarding the FDR, and Andy Gould for suggesting the importance of follow-up observations of the stars that flared. We are grateful to John Wisniewski for sharing APO 3.5 m observing time with us. A.F.K., S.L.H., and E.J.H. acknowledge support from NSF grant AST 08-07205. J.J.B. and S.L.H. acknowledge support from NSF grant AST 06-07644. A.C.B. acknowledges support from NASA grant NNX09AC77G.

Funding for the SDSS and SDSS-II has been provided by the Alfred P. Sloan Foundation, the Participating Institutions, the National Science Foundation, the U.S. Department of Energy, the National Aeronautics and Space Administration, the Japanese Monbukagakusho, the Max Planck Society, and the Higher Education Funding Council for England. The SDSS Web site is http://www.sdss.org/.

The SDSS is managed by the Astrophysical Research Consortium for the Participating Institutions. The Participating Institutions are the American Museum of Natural History, Astrophysical Institute Potsdam, University of Basel, University of Cambridge, Case Western Reserve University, University of Chicago, Drexel University, Fermilab, the Institute for Advanced Study, the Japan Participation Group, Johns Hopkins University, the Joint Institute for Nuclear Astrophysics, the Kavli Institute for Particle Astrophysics and Cosmology, the Korean Scientist Group, the Chinese Academy of Sciences (LAMOST), Los Alamos National Laboratory, the Max-Planck-Institute for Astronomy (MPIA), the Max-Planck-Institute for Astrophysics (MPA), New Mexico State University, Ohio State University, University of Pittsburgh, University of Portsmouth, Princeton University, the United States Naval Observatory, and the University of Washington.

REFERENCES

Abazajian, K. N., et al. 2009, ApJS, 182, 543
Adelman-McCarthy, J. K., et al. 2008, ApJS, 175, 297
Audard, M., Güdel, M., Drake, J. J., & Kashyap, V. L. 2000, ApJ, 541, 396
Becker, A. C., et al. 2004, ApJ, 611, 418
Binney, J., Gerhard, O., & Spergel, D. 1997, MNRAS, 288, 365
Blanton, M. R., et al. 2005, AJ, 129, 2562
Bochanski, J. J., Munn, J. A., Hawley, S. L., West, A. A., Covey, K. R., & Schneider, D. P. 2007a, AJ, 134, 2418
Bochanski, J. J., West, A. A., Hawley, S. L., & Covey, K. R. 2007b, AJ, 133, 531
Bochanski, J. J., Jr. 2008, PhD thesis, Univ. Washington
Chalabaev, A., & Maillard, J. P. 1983, A&A, 127, 279
Cohen, M. 1995, ApJ, 444, 874
Covey, K. R., Bochanski, J. J., Hawley, S. L., Davenport, J., Reid, I., & Golimowski, D. 2006, BAAS, 38, 940

Covey, K. R., Bochanski, J. J., Hawley, S. L., Davenport, J., Reid, I., & Golimowski, D. 2007, AJ, 134, 2398
Covey, K. R., Bochanski, J. J., Hawley, S. L., Davenport, J., Reid, I., & Golimowski, D. 2008a, AJ, 136, 1778
Covey, K. R., et al. 2008b, ApJS, 178, 339
Filippenko, A. V. 1982, PASP, 94, 715
Finkbeiner, D. P. 2003, ApJS, 146, 407
Finkbeiner, D. P., et al. 2004, AJ, 128, 2577
Fischer, D. A., & Marcy, G. W. 1992, ApJ, 396, 178
Frieman, J. A., et al. 2008, AJ, 135, 338
Fukugita, M., Ichikawa, T., Gunn, J. E., Doi, M., Shimasaku, K., & Schneider, D. P. 1996, AJ, 111, 1748
Giampapa, M. S., & Liebert, J. 1986, ApJ, 305, 784
Gizis, J. E., Reid, I. N., & Hawley, S. L. 2002, AJ, 123, 3356
Güdel, M., Audard, M., Kashyap, V. L., Drake, J. J., & Guinan, E. F. 2003, ApJ, 582, 423
Gunn, J. E., et al. 1998, AJ, 116, 3040
Gunn, J. E., et al. 2006, AJ, 131, 2332
Hawley, S. L., & Fisher, G. H. 1992, ApJS, 78, 565
Hawley, S. L., Gizis, J. E., & Reid, I. N. 1996, AJ, 112, 2799
Hawley, S., Reid, I. N., & Gizis, J. 2000, in ASP Conf. Ser. 212, From Giant Planets to Cool Stars, ed. C. A. Griffith & M. S. Marley (San Francisco, CA: ASP), 252
Hawley, S. L., Tourtellot, J. G., & Reid, I. N. 1999, AJ, 117, 1341
Hogg, D. W., Finkbeiner, D. P., Schlegel, D. J., & Gunn, J. E. 2001, AJ, 122, 2129
Ivezić, Ž., et al. 2004, Astron. Nachr., 325, 583
Ivezić, Ž., et al. 2007, AJ, 134, 973
Ivezić, Ž., et al. 2008, Serbian Astronomical Journal, 176, 1
Jurić, M., et al. 2008, ApJ, 673, 864
Kaiser, N. 2004, BAAS, 36, 828
Lacy, C. H., Moffett, T. J., & Evans, D. S. 1976, ApJS, 30, 85
McGehee, P. M. 2008, in Handbook of Star Forming Regions, Volume II: the Southern Sky, ed. B. Reipurth (San Francisco, CA: ASP), 813
Miller, C. J., et al. 2001, AJ, 122, 3492
Moffett, T. J. 1974, ApJS, 29, 1
Moore, A. 1999, in Advances in Neural Information Processing Systems, Vol. 11, ed. M. S. Kearns, S. A. Solla, & D. A. Cohen (Cambridge, MA: MIT Press), 543
Ng, Y. K., Bertelli, G., Chiosi, C., & Bressan, A. 1997, A&A, 324, 65
Oke, J. B., & Gunn, J. E. 1983, ApJ, 266, 713
Perryman, M. A. C., et al. 2001, A&A, 369, 339
Pettersen, B. R. 1988, in Astrophysics and Space Science Library 143, Activity in Cool Star Envelopes, ed. O. Havnes, J. E. Solheim, B. R. Pettersen, & J. H. M. M. Schmitt (Dordrecht: Kluwer), 49
Pier, J. R., Munn, J. A., Hindsley, R. B., Hennessy, G. S., Kent, S. M., Lupton, R. H., & Ivezić, Ž. 2003, AJ, 125, 1559
Reid, I. N., Gizis, J. E., & Hawley, S. L. 2002, AJ, 124, 2721
Reid, I. N., & Hawley, S. L. 2005, in New Light on Dark Stars, Red Dwarfs, Low-Mass Stars, Brown Stars, ed. I. N. Reid & S. L. Hawley (Chichester: Praxis Publishing)
Rockenfeller, B., Bailer-Jones, C. A. L., Mundt, R., & Ibrahimov, M. A. 2006, MNRAS, 367, 407
Schlegel, D. J., Finkbeiner, D. P., & Davis, M. 1998, ApJ, 500, 525
Smith, J. A., et al. 2002, AJ, 123, 2121
Smolčić, V., et al. 2004, ApJ, 615, L141
Soderblom, D. R., Duncan, D. K., & Johnson, D. R. H. 1991, ApJ, 375, 722
Stetson, P. B. 1996, PASP, 108, 851
Stoughton, C., et al. 2002a, AJ, 123, 485
Stoughton, C., et al. 2002b, AJ, 123, 485
Tucker, D. L., et al. 2006, Astron. Nachr., 327, 821
Tyson, J. A. 2002, Proc. SPIE, 4836, 10
Walkowicz, L. M., & Hawley, S. L. 2009, AJ, 137, 3297
Welch, D. L., & Stetson, P. B. 1993, AJ, 105, 1813
Welsh, B. Y., et al. 2007, ApJS, 173, 673
West, A. A., Hawley, S. L., Bochanski, J. J., Covey, K. R., Reid, I. N., Dhital, S., Hilton, E. J., & Masuda, M. 2008, AJ, 135, 785
West, A. A., Walkowicz, L. M., & Hawley, S. L. 2005, PASP, 117, 706
West, A. A., et al. 2004, AJ, 128, 426
Wielen, R. 1977, A&A, 60, 263
Wilson, O., & Woolley, R. 1970, MNRAS, 148, 463
York, D. G., et al. 2000, AJ, 120, 1579